Int. J. Therm. Sci. (2000) 39, 505–513

S1290-0729(00)00206-4/FLA

Onset of nucleate boiling in minichannels

Ingo Hapke, Hartwig Boye, Jürgen Schmidt *

Institute of Fluiddynamics and Thermodynamics, Otto-von-Guericke-University Magdeburg, PO Box 4120, D-39016 Magdeburg, Germany

(Received 24 June 1999, accepted 7 September 1999)

Abstract — Heat transfer characteristics during flow boiling in a minichannel were studied. For these investigations a thermographic measuring method was used. The axial distribution of the external wall temperature was measured, from which the internal wall temperatures and the local heat transfer coefficient are calculable. Detailed investigations were carried out in particular for the onset of nucleate boiling. The results of the measurements on a vertical evaporator pipe with an internal diameter of 1.5 mm are presented in dependence on the mass flux and the heat flux. A model for the prediction of the initial point of boiling and the wall-superheat has been derived based on the experiments. © 2000 Éditions scientifiques et médicales Elsevier SAS

nucleate boiling / onset nucleate boiling / heat transfer in boiling / minichannels / boiling in minichannels

Résumé — **Démarrage de l'ébullition nucléée en minicanaux.** On a étudié les caractéristiques du transfert de chaleur au cours de la vaporisation d'eau dans un minitube. Pour cela une méthode de mesure thermographique, qui est décrite, a été utilisée. On mesure la distribution axiale de la température à la surface externe, à partir de laquelle les températures internes de la paroi et les coefficients locaux de convection sont calculables. Les résultats des mesures pour un tube vertical de 1,5 mm de diamètre sont présentés en fonction de la densité de flux de chaleur et de masse. En particulier, on a réalisé des investigations détaillées pour analyser le début de l'ébullition. Basé sur les expériences, un modèle pour la détermination du point initial de l'ébullition et de la surchauffe de la paroi a été élaboré. © 2000 Éditions scientifiques et médicales Elsevier SAS

ébullition nucléée / démarrage de l'ébullition nucléée / transferts thermiques en ébullition / minicanaux / ébullition en minicanaux

Nomenclature

A	area	m^2
c_p	specific heat capacity	$J{\cdot}kg^{-1}{\cdot}K^{-1}$
d_h	hydraulic diameter	m
h	specific enthalpy	$J{\cdot}kg^{-1}$
h'	specific saturation enthalpy	$J{\cdot}kg^{-1}$
Δh_V	latent heat of vaporization	$J{\cdot}kg^{-1}$
k	correlation factor	
l_{ch}	characteristic length	m
l_u	unheated length of pipe	m
$\dot{M}$	mass flow	$kg{\cdot}s^{-1}$
$\dot{m}$	mass flux	$kg{\cdot}m^{-2}{\cdot}s^{-1}$
m	correlation factor	
N_b	number of boiling	
Nu	Nusselt number	
Ph	phase change number	
p	pressure	Pa
Pe	Péclet number	
Pr	Prandtl number	
$\dot{q}$	heat flux	$W{\cdot}m^{-2}$
$\dot{q}_V$	rate of energy generation per unit volume	$W{\cdot}m^{-3}$
r	radial distance	m
Re	Reynolds number	
St	Stanton number	
T	temperature	K
U	circumference	m
V	volume	m^3
v	specific volume	$m^3{\cdot}kg^{-1}$
w	velocity	$m{\cdot}s^{-1}$
z	coordinate in axial direction of tube	m
α	heat transfer coefficient	$W{\cdot}m^{-2}{\cdot}K^{-1}$
ε	emissivity	
λ	thermal conductivity	$W{\cdot}m^{-1}{\cdot}K^{-1}$
σ	surface tension	$N{\cdot}m^{-1}$
ϑ	temperature	°C

Subscripts

E	inlet of evaporator section

* Correspondence and reprints.
juergen.schmidt@vst.uni-magdeburg.de

el	electrical
env	environment
err	error
Fl	fluid
i, ini	initial point
in	inner
out	outer
G	gas
L	liquid
0	inlet
S	boiling state
W	wall

1. INTRODUCTION

The number of the investigations of heat and mass transfer in miniaturized channels has increased over the last few years.

On one hand, engineering applications of the microtechnique gain in importance, e.g., in automotive and process engineering, microelectronics as well as mechanical engineering and industrial manufacturing.

On the other hand, the governing laws of heat and mass transfer in mini- and microchannels differ essentially from those which apply to regularly dimensioned flow channels.

Peng and Wang [1] gave an overview of the state of knowledge in the field of single-phase forced convection and flow boiling in micro channels in 1998.

Starting with the work of Tuckmann and Pease in 1981 [2], the research on microchannels is a relatively young field of research. However, the great number of publications indicate that a considerable wealth of experience in the work with miniature channels has been gained. For example, a strong dependence of the heat transfer on the particular geometry of the flow channel was found while the hydraulic diameter was kept constant [1, 3]. Therefore, the specification of further geometrical conditions would be needed, e.g., the aspect ratios of a rectangular channel or the angles of a triangular channel.

Furthermore, changes in the flow character can be found even for critical Reynolds numbers of $Re = 200-700$ [1]. *Re* is based on the hydraulic diameter.

The determination of the flow regimes developed in a two-phase flow in dependence on the flow conditions is still considered to be problematic [4]. Compared to regularly dimensioned evaporator channels, the conditions for the beginning of boiling were found to be changed.

Peng and Wang [1] pointed out that the generation and growth of bubbles require a certain minimum of liquid space. If this is missing, boiling does not start if the conventional superheating of the liquid is given, and only micro steam bubbles can arise. This can only be visualized with special techniques.

Their hypotheses of the "Evaporating space" and of the "Fictitious boiling" indicate that a relatively high superheating of the liquid is necessary in order to start the boiling process.

Such increases in the superheating of the liquid compared to the initial point in regularly dimensioned evaporation channels are reported in [5].

These investigations were carried out for the transition zone from the conventionally dimensioned evaporator pipe $l_{ch} > 3$ mm to the micro channel $l_{ch} < 1$ mm. The phenomena determining the boiling in microchannels already have an influence on the processes in the pipes investigated.

The goal of the investigations presented was the derivation of a model of initial boiling in a minichannel based on extensive measurements.

This model should allow the prediction of both the location of the initial point of boiling in the evaporator channel and the wall-superheating required for the initialization of boiling.

2. EXPERIMENTAL METHOD

The experimental device is presented in *figure 1*. The reservoir (a) is filled with deionized water as the test fluid. The water was degassed in preparation for each experiment. This was achieved by heating the fluid to a temperature of 85 °C and keeping constant for a span of time of 2 hours. Its temperature can be set by means of the thermostat adjustment (b). The purpose of the gear pump (c) is to adjust the mass flow and to ensure the necessary preliminary pressure. The mass flow is measured by means of a flow meter (d) operating according to the Coriolis principle. After passing the test section (e) the fluid flows into the expansion container (f). The expansion container is connected to the atmosphere. The fluid in this container is at atmospheric pressure. Liquid not evaporated is returned to the reservoir (a).

A direct electric heating of the test section keeps the heat flux density on the wall constant.

The mass flux $\dot{m}$ and the heat flux $\dot{q}$ were varied within the ranges of $100 \leq \dot{m}[\mathrm{kg{\cdot}m^{-2}{\cdot}s^{-1}}] \leq 500$ and

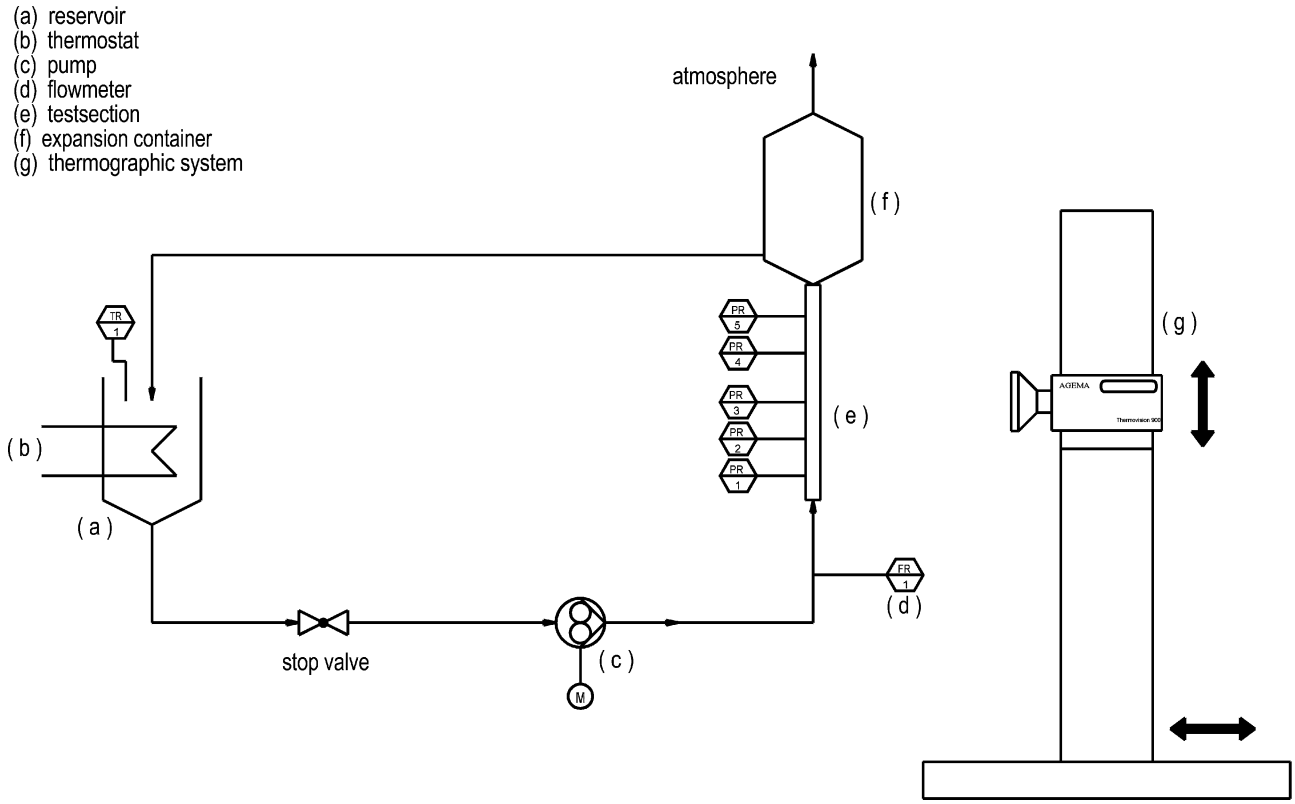

Figure 1. Sketch of the experimental apparatus.
Figure 1. Schéma du dispositif experimental.

$50 \leq \dot{q}[\mathrm{kW \cdot m^{-2}}] \leq 200$ in the experiments. The test section was a cylindrical tube made of the nickel based alloy 2.4816. The inner and outer diameter of the tube were $d_{\mathrm{in}} = 1.5$ mm and $d_{\mathrm{out}} = 3.0$ mm. The measured roughness has an order of magnitude of 5 μm. The flow direction was upwards.

A hydrodynamically stabilized flow at the entrance of the heated section is ensured by the upstream unheated first section. The unheated section has a length of $l_{\mathrm{u}} = 0.45$ m.

The axial distribution of the external wall temperature is measured using the thermography system AGEMA Thermovision 900 (g) [5]. This system is sensitive to radiation in the long wave spectrum of 8–12 μm. A 5° objective with an additional CLOSE-UP lens was used for the experiments. Thus, an area of 54 mm × 27 mm (full image mode) could be scanned when the camera was located at a distance of 0.6 m to the wall.

Figure 2 shows a thermographic image of a heated evaporator tube. The software of the system allows different modes of analysis. For example, the temperatures

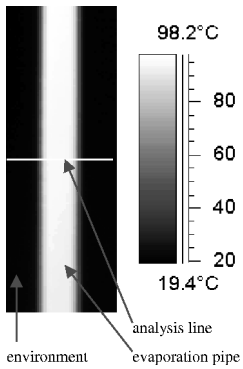

Figure 2. Thermographic image of the evaporation pipe.
Figure 2. Image thermographique du tube d'évaporation.

along a selected line can be scanned and statistically analyzed. Such an "analysis line" across the axis of the evaporator tube is demonstrated in *figure 2*. The pixel of the analysis line with the highest temperature indicates the temperature on the outer surface of the evaporator pipe.

The thermography system used allows the recording of image sequences. This renders the possibility of pre-

senting transient temperature fields. In order to observe the whole length of the evaporator pipe, the thermography system was moved vertically upward at constant velocity using a traverse device. Given the speed of the traverse device, the axial temperature distribution on the outer wall of the evaporation tube can be computed based on the temperature-versus-time plot for the point with the highest temperature of the analysis line.

The advantages of such an infrared measuring technique are the quasi-continuous, contactless temperature measurement and the almost delay-free registration of transient changes in temperature. However, one faces difficulties such as the inhomogeneities of the radiation properties of the wall of tube and the unprecise knowledge of the absolute values of the emissivities. The effect of an error in determining the emissivity on the precision of the temperature field can be analyzed by using the law of Stefan and Boltzmann:

$$\dot{e}(T) = \varepsilon\sigma_S T^4 = \varepsilon_{err}\sigma_S T_{err}^4 \qquad (1)$$

As a result of the incorrect emission value $\varepsilon_{err} = \varepsilon + \Delta\varepsilon$, the deviated temperature T_{err} differs from the real surface temperature T.

According to the relative error of the temperature measurement

$$\frac{T_{err} - T}{T} = \left(\frac{\varepsilon}{\varepsilon + \Delta\varepsilon}\right)^{1/4} - 1 \qquad (2)$$

small temperature measuring errors result in the case that the surfaces have an emissivity which approaches $\varepsilon = 1.0$. Therefore, the test section was coated uniformly with a special lacquer. An emissivity of approximately 0.94 resulted for these measurements. The temperature dependence of ε within the considered range can be neglected.

The local distribution of the emissivity, caused by the inhomogeneities of the lacquer coat, was determined by a calibration measurement. For that, the test section was used without heating. The test fluid flowed through the test section. The inlet temperature of the fluid was kept constant ($T_{Fl_E} > T_{env}$). In consideration of heat conduction in the wall and heat loss to the environment, the outer wall temperature can be calculated. The local emissivity can be determined by means of the known outer wall temperature and the measured temperature by using the thermography system.

For the analysis of the experiments, the inner wall temperature was calculated by using the solution of the heat conduction problem with the outer wall temperature measured as boundary condition. Usually quasi-stable conditions can be assumed.

However, local fluctuations of the temperature occur caused by the boiling process and by pressure fluctuations. An error occurs if the results of measurement of these temperature profiles are analyzed by the steady method. The size of this error was estimated by a simulation of the one-dimensional unsteady heat conduction problem. The inner wall temperature was given by a sinus-function similar to *figure 8*. The boundary condition on the outer wall surface is the boundary condition of the third kind. Subsequently, the inner wall temperature was determined with the solution of the one-dimensional steady state heat conduction problem with the outer wall temperature calculated by the unsteady state problem as a boundary condition. This inner wall temperature was compared to the inner wall temperature given as boundary condition by the unsteady state calculation. A small phase shift occurred. The deviations of the amplitudes can be neglected under the given experimental conditions.

Therefore, the measured outer wall temperatures can be converted to the inner wall temperatures, using the solution of one-dimensional heat conduction in steady-state if the assumption is allowed that the transient temperature changes are very small:

$$T_W = T_{in} = T_{out} - \frac{\dot{q}_V}{2\lambda}\left[r_{out}^2 \ln\frac{r_{out}}{r_{in}} - \frac{1}{2}\left(r_{out}^2 - r_{in}^2\right)\right] + \frac{\alpha_{out} r_{out}}{\lambda}(T_{out} - T_{env}) \ln\frac{r_{out}}{r_{in}} \qquad (3)$$

The physical properties are assumed to be constant. *Figure 3* shows the location of the temperatures.

The outer heat transfer coefficient α_{out} has to be measured. It consists of a convective and a radiative part. Its influence on T_{in} rises with decreasing values of the

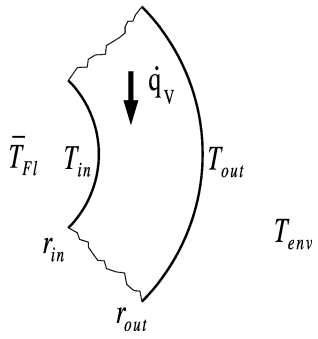

Figure 3. Section of pipe wall. Explanation of the nomenclature used.

Figure 3. Section de mur du tube. Illustration de la nomenclature utilisée.

heat flux into the evaporating liquid:

$$\dot{q} = \dot{q}_{\text{in}} = \dot{q}_{\text{V}} \frac{V}{A_{\text{in}}} - \frac{A_{\text{out}}}{A_{\text{in}}} \alpha_{\text{out}} (T_{\text{out}} - T_{\text{env}}) \qquad (4)$$

The radial heat conduction in the channel wall is superposed by the axial heat conduction, as confirmed by the wall temperature distribution presented in *figure 5*. A comparison between the one-dimensional and the two-dimensional calculation of the wall temperature is carried out in the area around the initial point. Therefore, the following differential equation can be applied:

$$\frac{1}{r} \frac{\partial}{\partial r} \left(r \lambda \frac{\partial T}{\partial r} \right) + \frac{\partial}{\partial z} \left(\lambda \frac{\partial T}{\partial z} \right) + \dot{q}_{\text{V}} = 0 \qquad (5)$$

Equation (5) was solved numerically for measured outer wall temperature distribution. Along the two edges in z-direction the boundary condition $\partial T / \partial z = \text{const}$ was set. The measured wall temperature distribution as well as the following boundary condition

$$-\lambda \left. \frac{\partial T}{\partial r} \right|_{\text{W,out}} = \alpha_{\text{out}} (T_{\text{out}} - T_{\text{env}}) \qquad (6)$$

were given at the outer wall of the tube.

Thus, the inner wall temperature can be computed in steady-state case. The difference between the one- and two-dimensional calculation is represented as an example in *figure 4*. There are large deviations only if the curvature of the temperature profile is very high.

With knowledge of the caloric average liquid temperature

$$\overline{T}_{\text{Fl}} = T_{\text{Fl}_{\text{E}}} + \frac{4\dot{q}}{\dot{m} c_p d_{\text{in}}} z \qquad (7)$$

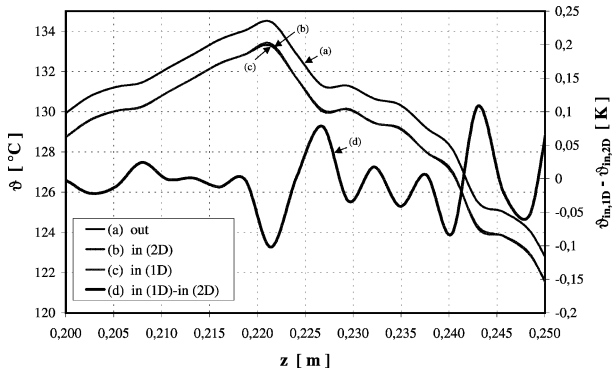

Figure 4. Comparison of results of one- and two-dimensional calculations of the inner wall temperature profile.

Figure 4. Distribution des températures à partir des calculs à une dimension en comparaison de celle obtenue par des calculs à deux dimensions.

the local heat transfer coefficient in the evaporator channel

$$\alpha = \frac{\dot{q}}{T_{\text{W}} - \overline{T}_{\text{Fl}}} \qquad (8)$$

can be determined.

3. RESULTS OF MEASUREMENT

The infrared system applied allows different scanning rates dependent on the size of image. Up to 30 pictures per second can be recorded in the half-image mode (272 × 68 pixels). As a typical result of such a measurement the axial wall temperature distribution is presented in *figure 5*.

The quasi-continuous axial temperature distributions are determined from sequences of thermographic images during a period of approximately 2 min.

In general, the typical tendencies of the major share of experiments are the following. The temperature reaches a maximum at the initial point after the single-phase liquid heating. A wall-superheating occurs at this point for the investigated minichannel. This superheating is essentially higher in wide ranges than those measured in larger dimensioned evaporator tubes if the same values of $\dot{q}$ and $\dot{m}$ are realized.

The relatively high wall or liquid superheatings initiate bubble formation processes at the initial point. They have different effects under the specific conditions of small channels.

On one hand, the steam bubble diameters can reach the order of magnitude of the channel dimension. This results, among other things, in increases in the pressure

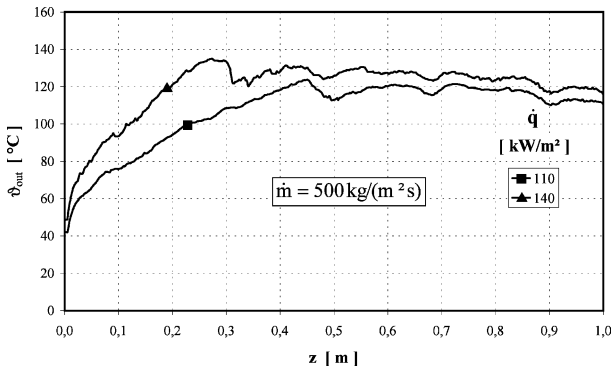

Figure 5. Measured temperature profiles as a function of the heat flux ($\varepsilon = \text{const}$).

Figure 5. Distribution des température mesurées en fonction de la densité de flux de chaleur.

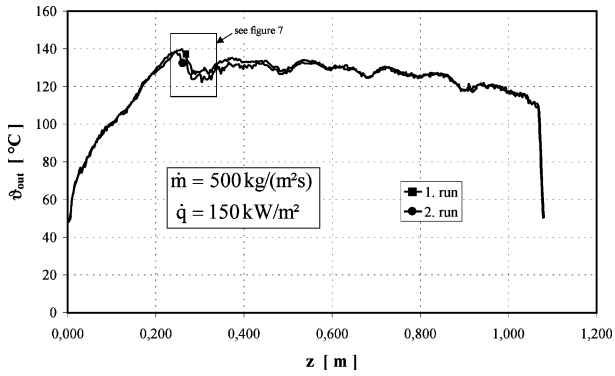

Figure 6. Axial temperature profiles (repeated measurements).
Figure 6. Distributions axiales de la température (essais répétés).

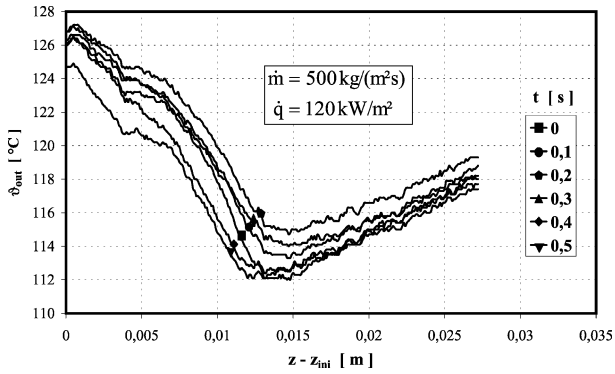

Figure 7. Time dependence of the temperature distribution near the initial point.
Figure 7. Distribution de la températures près du point initial en fonction du temps.

drop which influence the bubble detachment and the bubble frequency. Thus transient pressure and mass flow oscillations are induced. These oscillations are typical for the evaporation process in minichannels. Some experimental parameters (relatively large heat flux, relatively small mass flux) favor fluctuations in pressure and mass flux to a very high degree when the boiling process starts. The experimental results are influenced by these pressure and mass flux fluctuations. Multiple repetitions of the measurements were made to determine the uncertainty in the experimental results, see also *figure 6*.

On the other hand, the intensity of the heat transfer rises strongly by onset of the bubble formation at the initial point. As a result, the wall temperatures drop after the initial point in the known way and rise again in downstream direction.

Larger heat fluxes lead to an increase in the wall-superheating at the initial point.

The local temperatures vary near the initial point when the boiling process starts. In the other regions the time dependence of the temperature is very small. This is confirmed by the comparison of two experimental runs shown in *figure 6*. These transient variations in temperature in the region of the initial point can be resolved by using the line-scanning mode of the thermography system. A recording frequency of approximately 2 500 lines per second can be achieved if single lines (272 × 1 pixels) are recorded. The results of such recordings within the region of the initial point are presented in *figure 7*. Amplitudes of 2 K with a frequency of the variation in temperature of approximately 2 cycles per second are achieved. The functional development of the temperature oscillations as a function of the time is remarkable. While the changes in temperature at the initial point show a more

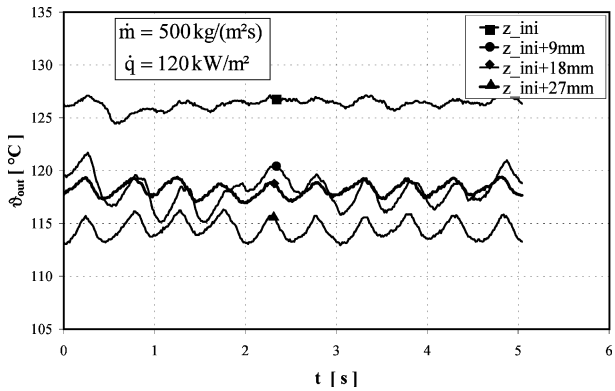

Figure 8. Oscillation of the wall temperature.
Figure 8. Oscillation de la température de mur.

or less statistical character, oscillating structures are generated downstream which approach harmonic functions, *figure 8*.

The recorded slow motion shots represent an excellent database for the effects of different flow mechanical and thermal conditions of the bubble development at the initial point which will be useful for further modeling.

4. INITIAL POINT— WALL-SUPERHEATING AND LOCATION

The results measured were compared with those of the equation of Sato and Matsumura as a physically founded

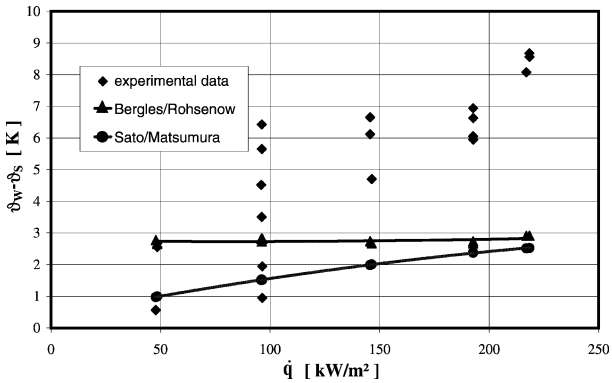

Figure 9. Comparison of measured wall-superheatings with the calculation results at the initial point.
Figure 9. Surchauffe du mur mesurée en comparaison de celle calculée au point initial.

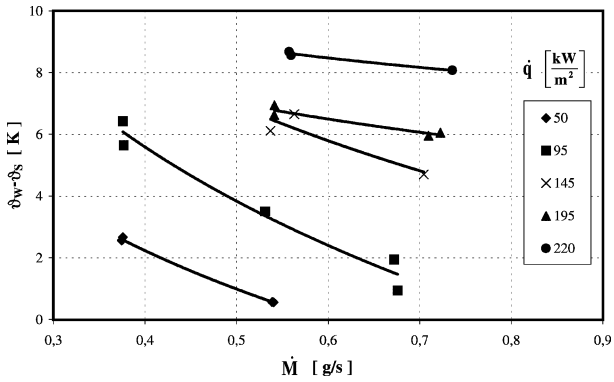

Figure 10. Mass flux dependence of the wall-superheating.
Figure 10. Influence du flux de masse sur la surchauffe de mur.

model [6]:

$$(T_W - T_S)_i = 2\left(\frac{2\sigma(v'' - v')T_S\dot{q}}{\Delta h_V \lambda'}\right)^{1/2} \tag{9}$$

as well as the empirical correlation of Bergles and Rohsenow [7]:

$$(T_W - T_S)_i = \frac{5}{9}\left(\left(\frac{\dot{q}}{1\,120}\right)^{0.463} p^{-0.535}\right)^{p^{0.0234}} \tag{10}$$

where p is given in bar. *Figure 9* shows the comparison of typical experimental data with the result of the computation using equations (9) and (10).

A satisfying agreement exists only for heat fluxes of about 50 kW·m^{-2}. However, the wall has to be superheated to a relatively great extent to initiate the nucleate boiling in the experiments for higher heat fluxes compared to models (9) and (10). A mass flux dependence of the wall-superheating occurs at the initial point, as shown in *figure 10*. Lower values of $(T_W - T_S)_i$ are measured for higher mass fluxes if the heat flux is constant. This tendency led to the derivation of a new correlation for the wall-superheating at the initial point with consideration of the mass flux dependence measured. This correlation is based on the number of boiling

$$N_b = \frac{\dot{q}}{\dot{m}\Delta h_V} \tag{11}$$

In known analyses of experimental investigations for normally dimensioned evaporator channels the characteristic phase number

$$Ph = \frac{h - h'}{\Delta h_V} \tag{12}$$

at the initial point is correlated with the number of boiling

$$-Ph_i = f(N_b) = kN_b^m \tag{13}$$

cf. Hodgson [8].

If one formulates a modified phase characteristic number

$$Ph_i^* = \frac{h_i - h_i'}{\Delta h_{V_i}} \tag{14}$$

with consideration of the saturation enthalpy and the enthalpy of evaporation under the pressure conditions at the initial point, follows

$$Ph_i^* = \left[\frac{c_p(\overline{T}_{Fl} - T_S)}{\Delta h_V}\right]_i = \left[\frac{c_p}{\Delta h_V}(\overline{T}_{Fl} - T_W)\left(1 - \frac{T_W - T_S}{T_W - \overline{T}_{Fl}}\right)\right]_i \tag{15}$$

Alternatively, the heat flux and the mass flux as well as the characteristic number N_b according to equation (11) and Stanton number $St = Nu/(RePr) = Nu/Pe$ can be introduced which results in

$$-Ph_i^* = \left[\frac{N_b}{St}\left(1 - \left(\frac{T_W - T_S}{T_W - \overline{T}_{Fl}}\right)\right)\right]_i \tag{16}$$

Assuming that the approach (13) is also valid for the modified characteristic phase number (14) and for laminar flow conditions, the relationship

$$\left(\frac{T_W - T_S}{T_W - \overline{T}_{Fl}}\right)_i = 1 - \left(St\,k N_b^{m-1}\right)_i = 1 - \left(St\frac{f(N_b)}{N_b}\right)_i \tag{17}$$

can be derived from equation (16).

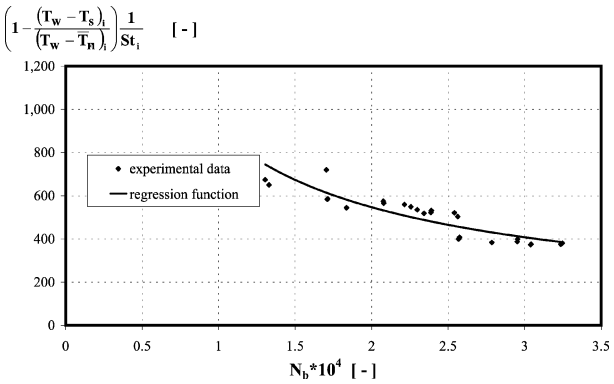

Figure 11. Dimensionless wall-superheating as a function of the boiling number.

Figure 11. Surchauffe de mur sans dimension en fonction du nombre d'ébullition.

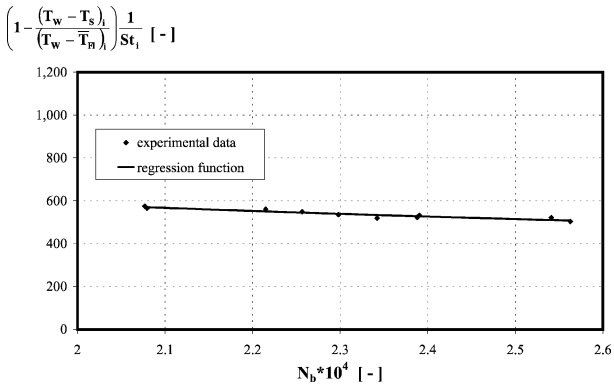

Figure 12. Dimensionless wall-superheating as a function of the boiling number, limited range.

Figure 12. Surchauffe de mur sans dimension en fonction du nombre d'ébullition, domaine limité.

Therefore, the wall-superheating required at the initial point depends on the pressure, on the technological parameters and on the Stanton number.

The experimental results are presented in *figure 11* as a function of boiling number, as follows:

$$\left[1-\left(\frac{T_W-T_S}{T_W-\overline{T}_{Fl}}\right)_i\right]\frac{1}{St}=\frac{f(N_b)}{N_b} \qquad (18)$$

The scattering range of the values measured, related to the regression function represented which includes all points registered, is caused by the unsteady state of the process.

The precision of the regression function can be increased in a small region of values of the heat fluxes. The regression results in the dependence

$$\frac{f(N_b)}{N_b}=5.1557N_b^{-0.555}, \qquad (19)$$

if the results of measurement are considered within the range $180 \le \dot{q}[\mathrm{kW\cdot m^{-2}}] \le 220$, *figure 12*. Thus the relation

$$-Ph_i^*=5.1557N_b^{0.445} \qquad (20)$$

can be derived.

As a result of the investigations a semi-empirical model is formulated which allows the iterative calculation of the wall-superheating at the initial point and the axial position of the initial point in the evaporator channel. The model indicated is restricted to vertical cylindrical tubes. The inlet temperature $T_{Fl_E}=40\,^{\circ}\mathrm{C}=\mathrm{const}$ was not varied in the experiments carried out, so that its influence is not considered in the model proposed. This possible influence must be investigated in further measurements.

The application of the model equation (20) to determine the location of the initial point and the wall-superheat at this point in dependence on the technological parameters $(\dot{q}, \dot{m})$ leads to an iteration procedure. The following steps have to be carried out:

1. Estimation of the axial position z_i.

2. Calculation of the caloric average temperature of the liquid at the location z_i using the energy balance (7), where $\overline{T}_{Fl_i}$ is the reference temperature for the material properties.

3. Computation of the characteristic numbers Pe_i, Nu_i and St_i.

The results are influenced by the kind of the determination of the Nu_i number. The heat transfer within the single-phase region near the initial point is intensified by the pressure and mass flux fluctuations in the evaporator pipe, by the transition from laminar to turbulent flows even at small *Re*, as well as by the developed bubbles at the active nucleation sites at the wall. The experimental values of the Nu_i number are compared with the calculated ones in *figure 13*. The correlation equation

$$Nu=4.36\left(1+\left(0.0292Pe\frac{d_h}{z}\right)^2\right)^{0.15}\left(\frac{Pr}{Pr_W}\right)^{0.14} \qquad (21)$$

for laminar flows used is described in [9].

The Nu_i values used to derive the model equation (20) are based on our own experimental results. In future Nu_i equations for the single-phase heat transfer in the vicinity of the initial point should be provided for practical application.

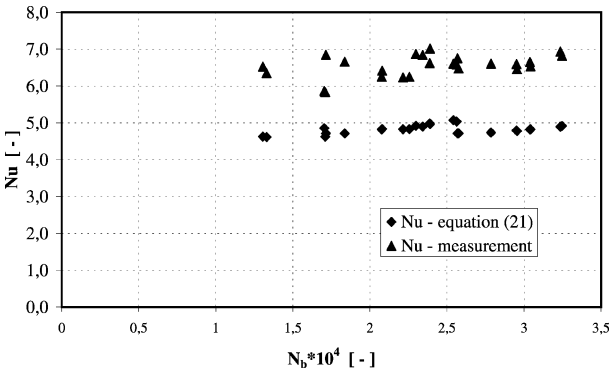

Figure 13. Comparison of the experimental *Nu* number at the initial point with the results achieved with single-phase equation after [9].

Figure 13. Nombres de Nusselt mesurés en comparaison de ceux déterminés par la corrélation pour la convection à une phase [9].

4. Calculation of the wall temperature using the single-phase heat transfer coefficient at the initial point according to equation (8).

5. Calculation of the boiling temperature at the initial point according to model equations (17) and (20)

$$T_{\mathrm{S_i}} = \left[T_{\mathrm{W}} - \left(1 - St\,k N_{\mathrm{b}}^{m}\right)\left(T_{\mathrm{W}} - \overline{T}_{\mathrm{Fl}}\right)\right]_{\mathrm{i}} \qquad (22)$$

Thus the wall-superheating is well-known.

6. Determination of the pressure at the initial point

$$p(z_{\mathrm{i}}) = f(T_{\mathrm{S_i}}) \qquad (23)$$

7. Calculation of the axial position of the initial point neglecting the flow pressure drop using Bernoulli's equation

$$z_{\mathrm{i}} = \frac{p_{\mathrm{E}} - p(z_{\mathrm{i}})}{\rho g} \qquad (24)$$

The values required of $(T_{\mathrm{W}} - T_{\mathrm{S}})_{\mathrm{i}}$ and z_{i} can be computed with an error of 10 % and 2 %, respectively, within the parameter interval where model (20) is valid.

The extension of the range of validity of the model (20) should be addressed in future works.

5. SUMMARY

Using the measuring method developed, the wall temperature of an evaporator channel can be measured in a quasi-continuous and contactless way. The local heat transfer coefficient can be calculated. This method was used especially for the investigation of the onset of nucleate boiling in minichannels.

The evaporation in the minichannel is characterized by relatively strong pressure and mass flux fluctuations. The resulting fluctuations of the wall temperatures could be measured in a mode allowing a high transient resolution of the images recorded. The transition of relatively statistical fluctuations of the wall temperature at the initial point to downstream temperature deviations approaching harmonic functions is remarkable.

The measured wall-superheatings at the initial point depend not only on the heat flux, but also on the mass flux. An semi-empirical model has been developed for the consideration of this additional dependence as the result of the measurements. It allows the prediction of the superheating of the wall at the initial point and of the location of the initial point in the evaporator channel for the geometry and boundary conditions considered in the experiment.

Acknowledgement

This work was supported by the Kultursministerium of the State Sachsen-Anhalt, Germany.

REFERENCES

[1] Peng X.F., Wang B.X., Forced-convection and boiling characteristics in microchannels, in: Proceedings of 11th International Heat Transfer Conference, Kyongju, Korea, Vol. 1, 1998, pp. 371–390.

[2] Tuckmann D.B., Pease R.F., High-performance heat sinking for VLSI, IEEE Electronic Device Letters EDL-2 (5) (1981) 126–129.

[3] Merker G.P., Konvektive Wärmeübertragung, Springer-Verlag, Berlin 1987.

[4] Lin S., Kew P.A., Cornwell K., Two-phase flow regimes and heat transfer in small tubes and channels, in: Proceedings of 11th International Heat Transfer Conference, Kyongju, Korea, Vol. 2, 1998, pp. 45–50.

[5] Hapke I., Boye H., Schmidt J., Staate Y., Investigation of flow boiling in minichannels using thermography, in: Eurotherm 57, Microscale Heat Transfer, Poitiers, 1998 (in print).

[6] Sato T., Matsumura H., On the conditions of incipient subcooled boiling with forced convection, Bulletin ISME 7 (26) (1963) 392–398.

[7] Bergles A.E., Rohsenow W.M., The determination of forced-convection surface boiling heat transfer 3, Heat Transfer 86 (1964) 365–372.

[8] Hodgson A.S., Forced convection subcooled boiling heat transfer with water in an electrically heated tube at 100 to 550 lb/in, Trans. Instn. Chem. Engrs. 46 (1968) 25–31.

[9] VDI-Wärmeatlas, 8. Auflage, Springer-Verlag, Berlin, 1997, Abschn. Hba3.